Anterior Lamina Cribrosa Surface Depth, Age, and Visual Field Sensitivity in the Portland Progression Project

Ruojin Ren,[1,2] Hongli Yang,[1] Stuart K. Gardiner,[3] Brad Fortune,[3] Christy Hardin,[1] Shaban Demirel,[3] and Claude F. Burgoyne[1]

[1]Devers Eye Institute, Optic Nerve Head Research Laboratory, Legacy Research Institute, Portland, Oregon
[2]Einhorn Clinical Research Center, Moise and Chella Safra Advanced Ocular Imaging Laboratory, New York Eye and Ear Infirmary of Mount Sinai Health System, New York, New York
[3]Devers Eye Institute, Discoveries in Sight Research Laboratories, Legacy Research Institute, Portland, Oregon

Correspondence: Claude F. Burgoyne, Optic Nerve Head Research Laboratory, Devers Eye Institute, Legacy Research Institute, 1225 NE 2nd Avenue, Portland, OR 97208-3950; cfburgoyne@deverseye.org.

RR and HY contributed equally to the work and should therefore be regarded as equivalent authors.

Submitted: October 3, 2013
Accepted: January 13, 2014

Citation: Ren R, Yang H, Gardiner SK, et al. Anterior lamina cribrosa surface depth, age, and visual field sensitivity in the Portland Progression Project. *Invest Ophthalmol Vis Sci*. 2014;55:1531-1539. DOI:10.1167/iovs.13-13382

Purpose. To assess the effect of age on spectral-domain optical coherence tomography (SDOCT)-detected lamina cribrosa depth while controlling for visual field (VF) status and retinal nerve fiber layer thickness (RNFLT) in 221 high-risk ocular hypertension and glaucoma patients enrolled in the Portland Progression Project.

Methods. In this cross-sectional study, each participant underwent 870-nm SDOCT to obtain high-resolution radial B-scans centered on the optic nerve head (ONH) and a standardized ophthalmologic examination, including automated perimetry, on the same day. For each ONH, an anterior lamina cribrosa surface depth (ALCSD) parameter was generated as the average perpendicular distance from each anterior lamina cribrosa surface point relative to Bruch's membrane opening (BMO) reference plane within all 24 delineated B-scans. The relative effects of age, age-corrected VF status (mean deviation [MD]), and RNFLT on ALCSD were analyzed.

Results. The mean age ± SD of participants was 64 ± 11 years (range, 33–90 years). The relationship between ALCSD and MD was age-dependent. ALCSD = 407.68 − 67.13 × MD − 0.08 × Age + 0.89 × MD × Age (MD, $P = 0.001$; MD × Age, $P = 0.004$). The relationship between ALCSD and RNFLT may also be age-dependent but did not achieve significance (interaction term, $P = 0.067$). ALCSD increased with worse VF status in younger eyes but not in older eyes. In older eyes, the anterior lamina was shallower than in younger eyes for the same VF status and RNFLT.

Conclusions. These data are consistent with the concept that structure/structure and structure/function relationships change with age.

Keywords: laminar depth, age, glaucoma, retinal nerve fiber layer thickness, visual field sensitivity

Glaucoma is a progressive optic neuropathy that results in structural changes in the optic nerve head (ONH) and retinal nerve fiber layer (RNFL), as well as specific patterns of functional abnormality within the visual field (VF) that may eventually lead to severe visual impairment and blindness.[1] A variety of data suggest that the optic nerve becomes more susceptible to progressive glaucomatous damage as it ages. In population-based studies,[2–5] age is an independent risk factor for both the prevalence of the neuropathy[2] and its progression,[3–5] regardless of the stage of damage. However, the clinical appearance of glaucomatous structural alterations in the aged ONH has characteristic features, which, in their most recognizable forms, are described as "senile sclerotic cupping."[6,7] This is typically a shallow form of "cupping" with greater pallor accompanied by more extensive peripapillary atrophy at all stages of VF loss than the deeper forms of cupping that are most common in the eyes of children or young adults.[6–13]

We have previously proposed that the "shallow" or "senile sclerotic" cupping of aged eyes is, in part, a manifestation of an increase in the structural stiffness of their ONH and peripapillary scleral connective tissues.[14,15] The structural stiffness of a tissue is determined by the combination of its geometry (arrangement and amount) and its constituent material properties (whether they are compliant like rubber or stiff like steel). We have also predicted that age-related differences in ONH connective tissue structural stiffness[16–25] should result in age-related differences in structure/structure (ONH/RNFL) and structure/function (ONH/VF) relationships[14,15]: specifically, that the magnitude of laminar deformation associated with a given VF status should be greater in young eyes (or "compliant" eyes of all ages) than in old eyes (or "stiff" eyes of all ages).[14,15] This concept is important because it may contribute to the emerging explanations for why the relationship between structural and functional changes might be specific to individual eyes and not necessarily predictable for all eyes.[26]

ONH structural changes in glaucoma include connective tissue deformation[27–37] and/or remodeling[38,39] in addition to gliotic changes[40] and retinal ganglion cell (RGC) axonal injury and loss.[15] Connective tissue deformation in glaucoma is more complicated than previously considered because of the dynamic interplay among the sclera, the scleral canal wall, and the lamina cribrosa[41–43] and because these phenomena

may change with age and disease stage. However, the following findings have been described in human and experimental glaucoma: peripapillary scleral bowing,[35] scleral canal and neural canal expansion,[30,33] posterior deformation,[27–29,31,37] initial thickening,[37] subsequent thinning,[27,28] and outward migration[39] of the lamina cribrosa.

Our specific hypothesis for this study was that, for a given level of IOP exposure, ONH structural changes in young eyes will be a manifestation of more posterior laminar deformation than RGC axon loss. Thus, ONH structural deformation in young eyes, characterized in terms of the depth of the anterior lamina cribrosa surface (ALCS) relative to Bruch's membrane opening, will likely be greater for a given amount of functional change and be associated with less RNFL loss than would the same amount of laminar deformation in older eyes. Stated differently, for a similar level of IOP exposure, the lamina will be less posteriorly deformed in older eyes than in younger eyes and for a given amount of laminar deformation will be associated with a greater amount of RNFL and functional loss.

The potential to tease apart neural and connective tissue components of the glaucomatous ONH and retina has improved due to the advent of spectral-domain optical coherence tomography (SDOCT) imaging.[44–48] In this cross-sectional study, we used SDOCT imaging to characterize anterior lamina cribrosa surface depth (ALCSD)[46] relative to a Bruch's membrane opening (BMO) reference plane in 1 eye each of 221 high-risk ocular hypertension and glaucoma patients enrolled in the Portland Progression Project. We then assessed the effect of age on ALCSD while controlling for IOP and 2 surrogates for stage of glaucomatous damage: VF status and RNFL thickness (RNFLT).

Subjects and Methods

Data for this study were obtained from the Portland Progression Project (P3 study),[49] a National Institutes of Health (NIH)-funded longitudinal study of progression in participants with high-risk ocular hypertension and glaucoma based at the Devers Eye Institute in Portland, Oregon. The protocol was approved by the Legacy Health Institutional Review Board. The study adheres to the tenets of the Declaration of Helsinki and complies with the Health Insurance Portability and Accountability Act of 1996. All participants provided written informed consent after having the risks and benefits of participation explained to them.

At study entry participants had either early glaucoma with VF loss less severe than –6 dB for mean deviation (MD) or ocular hypertension (untreated IOP greater than 22 mm Hg) plus 1 or more risk factors for the presence or progression to glaucoma as determined by their clinician. Risk factors for the presence or progression to glaucoma included age $>$ 70 years, systemic hypertension, migraine, diet-controlled diabetes, peripheral vasospasm, African ancestry, self-reported family history of glaucoma, and suspicious ONH appearance (cup-to-disc ratio asymmetry $>$ 0.2, neuroretinal rim notching, or narrowing or disc hemorrhage). All participants also met the following criteria for both eyes: best corrected visual acuity of 20/40 or better and spectacle refraction less than $\pm$5.00-diopter (D) sphere and less than $\pm$2.00-D cylinder. Potential participants were excluded if they had any previous or current ocular or neurologic disease likely to affect the VF and previous ocular surgery (except uncomplicated cataract surgery).

SDOCT ONH imaging was introduced into the P3 imaging protocol in 2009, at which point a subset of subjects had progressed to more advanced stages of VF loss. For the current study, only SDOCT data from the baseline SDOCT ONH imaging session or the nearest session in which acceptable VF testing was available were included. In addition to SDOCT ONH and RNFL imaging, all participants underwent standard automated perimetry and IOP measurement by Goldmann applanation tonometry on the same day.

SDOCT and Visual Field Data Acquisition

Data from 1 eye of each participant were included. For each participant, the eye with the best qualitative SDOCT laminar visualization was chosen. In those participants in whom SDOCT laminar visualization was qualitatively similar in both eyes, 1 eye was randomly selected.

Standard automated perimetry VF testing was performed using a Humphrey Field Analyzer II (Carl Zeiss, Meditec, Inc., Dublin, CA) using the 24-2 testing pattern and conventional test procedures. All tests used the Swedish interactive thresholding algorithm (SITA)-standard threshold strategy.[50] An optimal lens correction was placed before the tested eye, and the fellow eye was occluded with a white plastic eye patch. All participants had previous experience with VF testing prior to entering the study, and most had undergone multiple VF tests prior to the first session, in which SDOCT ONH imaging was also performed. Only reliable VFs were included, defined as $\leq$30% false negatives and fixation loss and $\leq$20% false positives. If fixation loss was $>$30%, then a note from the technician confirming that fixation was observed to be stable throughout the test could override the blind spot monitor report, as fixation losses can be erroneously reported when the perimeter's initial mapping of the blind spot is inaccurate. The MD index was used to characterize the functional status.

SDOCT imaging was performed using a standard Spectralis unit (Heidelberg Engineering, GmbH, Heidelberg, Germany) with an 870-nm source. A radial scanning pattern visually centered on the ONH by the technician was used to obtain 48 high-resolution radial B-scans over a 15° area (768 A-scans per B-scan), as seen in Figure 1. The device's eye-tracking capability was used during image acquisition to enable B-scan sweep averaging ($n = 9$) in real time to reduce speckle noise.[51] All acquired SDOCT scans had a quality score better than 15.

SDOCT Image Delineation

Our strategy for SDOCT ONH image delineation has been described in a series of previous reports.[46,47,52] Raw SDOCT volumes were exported into our custom-made "multiview" three-dimensional (3D) visualization and delineation software based on the Visualization Toolkit (VTK, Clifton Park, NY). ONH and peripapillary RNFL landmarks were then manually delineated within every second radial B-scan (24 total) of each SDOCT volume (Fig. 1). Two operators (RR and CH), who were masked to all other participant information, performed all of the delineations. Delineated landmarks (Fig. 1) included the internal limiting membrane (ILM); the posterior surface of the RNFL and posterior surface of the Bruch's membrane/retinal pigment epithelium (BM/RPE) complex; the BMO (defined as the innermost termination of the SDOCT-detected BM/RPE on either side of neural canal); and the ALCS.

In the case of the ILM, RNFL, and BM/RPE complex, each surface was delineated using discrete points connected by a Bézier curve. Within each radial B-scan, delineated points for each landmark were finely adjusted so that the fitted Bézier curve most closely matched the anatomy. The strategy for delineating the ALCS was based on our previous direct comparisons between SDOCT B-scans and matched histologic sections obtained from a normal non-human primate eye,[47] as well as our previous publications on SDOCT longitudinal change detection[46] and enhanced depth versus standard SDOCT imaging.[52] Within each B-scan, we identified the ALCS

Investigative Ophthalmology & Visual Science

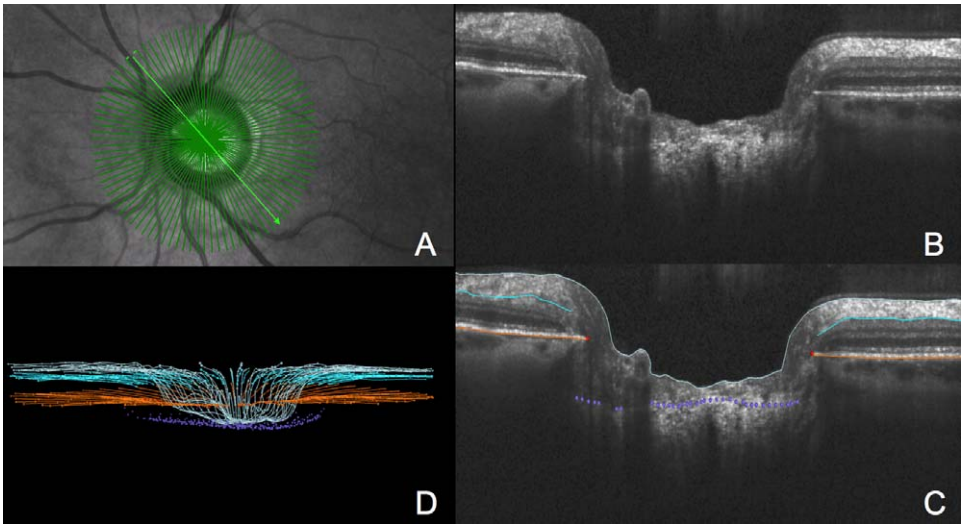

Figure 1. Settings were 15° scan, 48 radial B-scans, 768 A-scans/B-scan, and each B-scan was the average of $n = 9$ repetitions. (**A**) IR image shows 48 radial B-scan pattern overlay. (**B**) Representative B-scan as described in the legend to (**A**). (**C**) Delineated B-scan shown in (**B**). *Light blue lines* indicate the ILM, *turquoise lines* the posterior surface of the RNFL, *orange lines* are the posterior surface of the BM/RPE complex, *red points* are the BMO, and *purple points* are the ALCS. (**D**) Point cloud of delineated points from the 24 radial B-scans that were delineated as a subset (see Subjects and Methods).

as being the most anterior point where a horizontally oriented, high-intensity signal below the disc surface intersected the high-intensity vertical striations we previously identified to be the prelaminar glial columns (Fig. 2). It is important to note that the ability to see the ALCS was diminished in regions where there was pronounced shadowing from overlying retinal vessels. For this reason, the ALCS was delineated using discrete marks rather than using continuous Bézier curves, and the delineators could use any number of marks, at their discretion, to delineate the ALCS. For each SDOCT volume, the best fitting spline through the 48 delineated BMO points was used to define the reference plane (BMO reference plane).[46,47,52,53] The following parameters were then calculated as single values for each SDOCT scan based on the BMO best-fit ellipse: BMO area, BMO major (maximum diameter), and BMO minor (minimum diameter).

Quantification of the Extent of ALCS Delineation

We previously described our method for quantifying the extent of ALCS delineation (MatLab; MathWorks, Natick, MA) (Fig. 2).[46,47,52] All delineated BMO and ALCS points were projected onto the BMO reference plane. The projected BMO points were connected by a B-spline.[33,52,53] The BMO B-spline, along with all of the contained projected ALCS points were converted to unit circle space and divided into a grid of 72 equal area sectors by using concentric rings and radial lines (Fig. 2). BMO sectors containing 2 or more projected ALCS points were considered delineated and included in the analysis. BMO sectors containing less than 2 projected ALCS points were excluded. After this point-filtration step, the unit circle space was converted back to the original projected BMO point B-spline configuration (Fig. 2).

ONH and RNFL Parameterization in Each SDOCT Volume

The ALCSD parameter was defined as the average perpendicular distance from each ALCS point relative to the BMO reference plane included within the 24 delineated B-scans of each ONH (Fig. 3). However, the delineated ALCS points were "weighted" so that points in the peripheral lamina contributed greater weight to the mean than those in the central portion of the lamina.[46] This was done because the points in the peripheral part of the lamina represent a "wider" arc than those toward the BMO centroid (i.e., the area of the ALCS

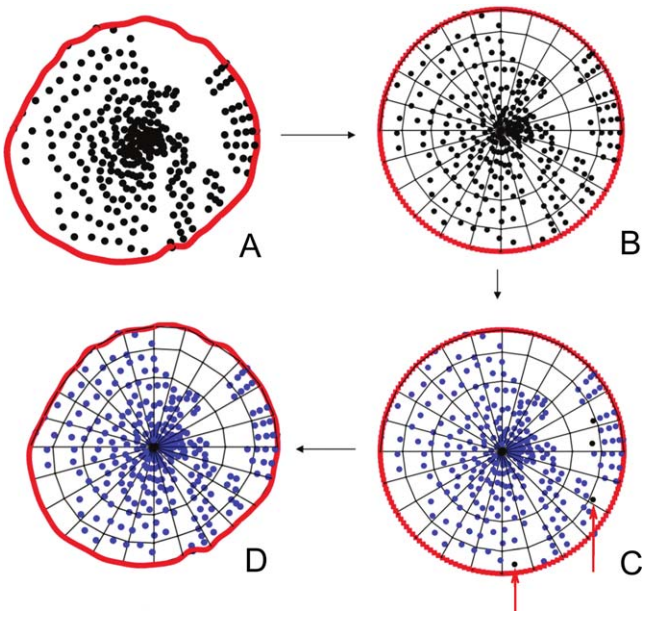

Figure 2. Method of ALCS point filtration and sector quantification are shown. (**A**) The ALCS points (*black glyphs*) are projected onto the plane (BMO reference plane) of a BMO B-spline (*red circle line*) best fitted to the BMO delineations. (**B**) The BMO B-spline is scaled into the unit circle space and subdivided into 72 sectors of equal area. (**C**) Sectors where 2 or more ALCS-delineated points are present in each volume are maintained for analysis. Sectors where there are fewer than 2 delineated points (*black glyphs* highlighted by *red arrows*) in each volume are filtered out of the analysis. (**D**) The circle is transformed back to its original space, with the filtered ALCS points removed.

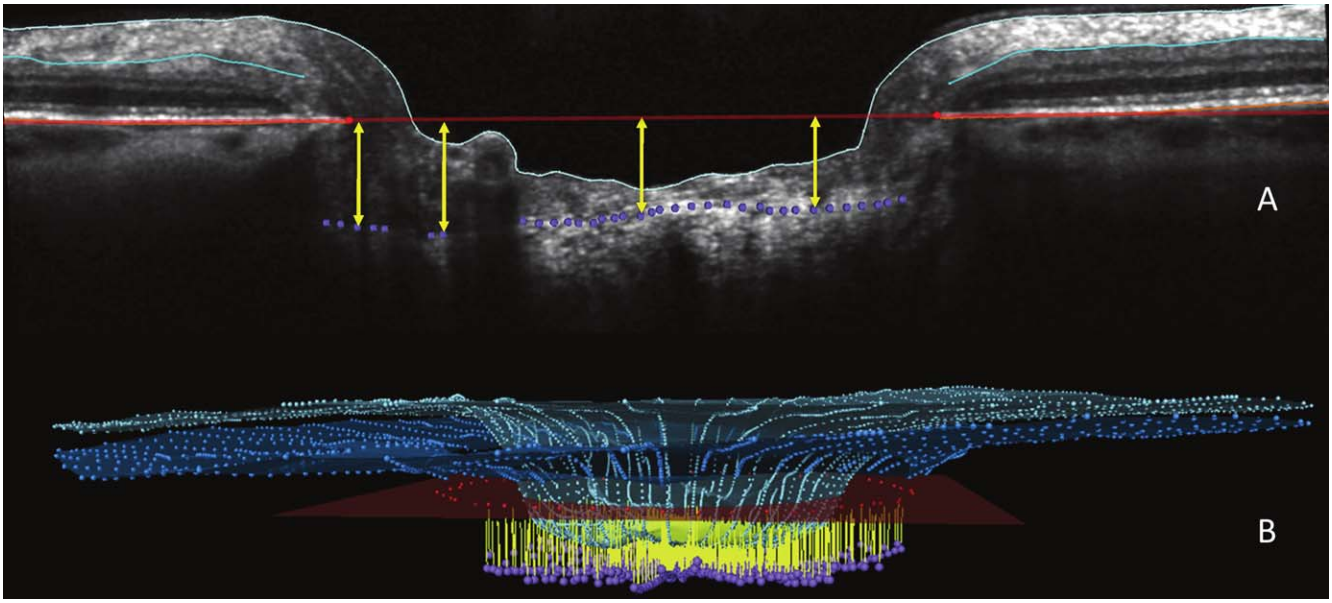

FIGURE 3. ALCSD measurement is shown. (**A**) ALCSD (*yellow arrows*) was quantified as the perpendicular distance from each delineated ALCS point to BMO reference plane (seen in cross-section as a *red line*) that met the criteria for inclusion (Fig. 2). (**B**) Mean ALCSD was the average of all ALCSD measurements (*yellow*) in 3D space for the 24 radial B-scans that were delineated for each ONH. The ILM (*light blue*) and outer RNFL (*turquoise*) are also shown.

wedge represented by a given point increases with the distance that point is from the BMO centroid). The weightings for each delineated point were thus proportional to the distance from the BMO centroid. SDOCT RNFLT was calculated at an eccentricity of 1700 μm (3.4-mm diameter) from the BMO centroid as previously described[46,52,54] and reported as the average minimum distance between the ILM and the posterior surface of the RNFL at 1700-μm eccentricity from the BMO centroid within the 24 delineated B-scans of each ONH (Fig. 4).

To increase the likelihood that we were making comparisons between the most posterior portions of the ALCS within all study eyes, we calculated 3 additional ALCSD parameters for each study eye. $ALCSD_{max1}$ was defined as the mean ALCSD value from the top 10% of all ALCSD values; $ALCSD_{max2}$ was defined as the mean ALCSD value from those BMO sectors containing the top 5% of all ALCSD values; and $ALCSD_{central}$ was defined as the mean ALCSD values from the center-most third of the projected ALCS sectors.

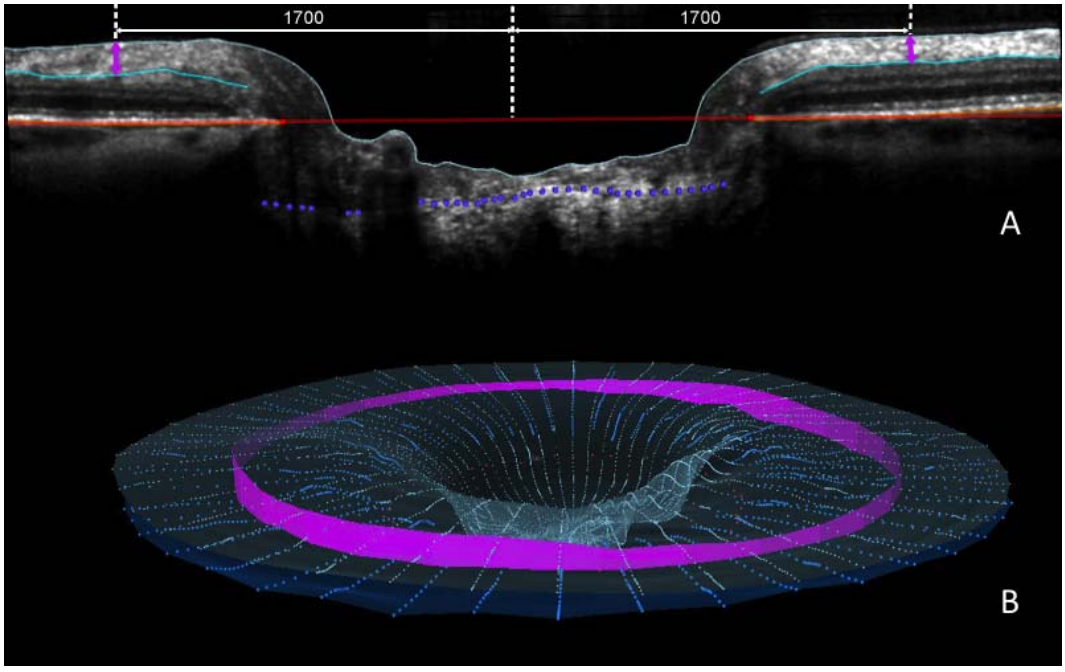

FIGURE 4. RNFLT measurement is shown (*pink band*). (**A**) RNFLT was measured on either side of the canal at ILM points that are 1700 μm (3.4-mm diameter) from the centroid of the 48 delineated BMO points (the BMO centroid). The perpendicular projection of the BMO centroid is shown as the central *white vertical dotted line*. RNFLT at each ILM point is the minimum distance (*pink arrow*) between the ILM and the posterior RNFL boundary (*turquoise* B-spline *line*). (**B**) 3D representation of interpolated RNFLT (*pink band*) is based on the 24 delineated B-scans.

Investigative Ophthalmology & Visual Science

Statistical Analysis

Statistical analyses were performed using the R software (R Foundation for Statistical Computing, Vienna, Austria). Clinical parameters and general ONH/RNFL outcome parameters (Table) are means ± standard deviations. Univariate least-squares regression models were formed to predict ALCSD from age and ALCSD from IOP. Multivariate models were constructed to assess the effects of age, MD, and their interactions on ALCSD, $ALCSD_{max1}$, $ALCSD_{max2}$, and $ALCSD_{central}$.

Univariate least-squares regression models were also formed to predict RNFLT from age and ALCSD from RNFLT. Multivariate models were constructed to assess the effects of age and RNFLT, and their interactions on ALCSD. Finally, the relationships using each of the 3 alternative definitions of ALCSD with RNFLT and age were assessed with univariate least-squares regression models and multivariate models.

Results

This cross-sectional study assessed 227 eyes of 227 participants. Six eyes were excluded from analysis because of poor ALCS visibility. Therefore a total of 221 of 227 eyes (97%) were included for analysis, ranging in age from 33 to 90 years old (mean ± SD age, 64 ± 11 years). Almost all participants were Caucasian (212 of 221, 96%) with 91 (41%) being male. The right eye was selected for 112 (51%) individuals. The demographics and clinical characteristics of the participants, together with their ALCSD and RNFLT data are summarized in the Table. Mean ± SD ALCSD was 405 ± 119 μm (range, 178–835 μm). Mean RNFLT was 89 ± 16 μm (range, 36–122 μm).

The mean number of delineated ALCS sectors for an eye (from a total of 72 [Fig. 2]) was 40 ± 13 (range, 13–72). Among the central 24 sectors, the mean ± SD number of delineated ALCS sectors was 20 ± 5 (range, 3–24). The percentage of ALCS projected area delineated was 56 ± 18% (range, 18%–100%). While the extent of nondelineated ALCS projected area was variable among participants, in most eyes it generally corresponded to the location of the central retinal vasculature.

Figures 5 and 6 show that the association between ALCSD and MD is age-dependent. The regression equation for ALCSD was $ALCSD = 407.68 - 67.13 \times MD - 0.08 \times Age + 0.89 \times MD \times Age$. Whereas both the MD ($P = 0.001$) and the MD × Age ($P = 0.004$) terms achieved significance, the Age term did not ($P = 0.921$). There was no significant univariate association between ALCSD and age ($P = 0.504$) or ALCSD and IOP ($P = 0.222$). These results indicate the following relationships within the data: first, ALCSD tends to be greater (deeper) with worse VF status (i.e., when MD is more negative) because the coefficient associated with the MD term (–67.13) makes the product (–67.13 × MD) progressively more positive. Second, this effect is lessened as age increases because the (0.89 × MD × Age) term becomes more negative with advancing age, reducing (shallowing) the ALCSD.

Figure 5 plots ALCSD against age, with points shaded according to their MD (darker points indicate worse MD). Two examples of regression lines are shown based on the equation given above. The solid gray line (Fig. 5) represents the relationship between ALCSD and age when MD = 0 dB. The dashed gray line (Fig. 5) represents the same relationship when MD = –10 dB. These examples suggest that among eyes with no detectable VF loss, there are no significant differences between the ALCSD of young and those of old eyes. However, among eyes with a given amount of VF loss (in this case –10 dB), the anterior lamina surface is deeper in younger eyes than in older eyes. Note that most cases with worse VF status (darker shaded symbols) are located to the right (older eyes) and toward the top (eyes with relatively shallow lamina cribrosa) of the scatterplot.

Table. Characteristics of the 221 Participants and the 221 Eyes in the Study

Characteristic	Mean ± Standard Deviation	Range
Age, y	64.3 ± 11.0	33.0–90.0
Intraocular pressure, mm Hg	17.4 ± 3.5	5.0–29.0
Mean deviation, dB	−0.69 ± 2.94	−16.53–3.29
ALCSD, μm	405 ± 119	178–835
SDOCT RNFLT, μm	89 ± 16	36–122
BMO area, mm^2	1.85 ± 0.43	1.03–3.20
BMO major, μm	1619 ± 186	1173–2169
BMO minor, μm	1442 ± 173	1083–1929

ALCSD, anterior lamina cribrosa surface depth; BMO, Bruch's membrane opening; RNFLT, retinal nerve fiber layer thickness; SDOCT, spectral-domain optical coherence tomography.

Figure 6 plots ALCSD against MD, with points shaded according to their age (darker symbols indicate older subjects). In this case, the two example lines (Fig. 6) show the relationship between ALCSD and MD at age 55 (Fig. 6, solid gray line) and age 75 (Fig. 6, dashed gray line). Note that in older eyes (here, age 75) ALCSD is unrelated to the VF status. However, among younger eyes (here, age 55), ALCSD is deeper when the status of the VF is worse.

Univariate correlations among 3 additional ALCSD parameters that were designed to more fairly compare laminar position among the study eyes ($ALCSD_{max1}$, $ALCSD_{max2}$, and $ALCSD_{central}$) and the 3 outcome parameters (age, IOP, and MD) were similar to those reported for ALCSD. Multivariate relationships among the 3 additional ALCSD parameters and MD were also age-dependent. The interaction term MD × Age was consistently significant, with $P = 0.007$, $P = 0.007$, and $P = 0.004$, respectively.

There was also a significant association between RNFLT and age such that $RNFLT = 112.26 - 0.37 \times Age$ ($P < 0.001$). There was no significant univariate association between RNFLT and ALCSD ($P = 0.225$) or between RNFLT and IOP ($P = 0.226$). If RNFLT was used as an indicator of "disease stage" instead of MD, then the regression equation describing ALCSD was $ALCSD = 1021.51 - 6.22 \times RNFLT - 8.38 \times Age + 0.08 \times RNFLT \times Age$ (RNFLT, $P = 0.040$; Age, $P = 0.047$; RNFLT × Age, $P = 0.067$). ALCSD was greater in eyes with a thinner RNFL, and this effect was again reduced in older than in younger eyes, as it was for MD. Moreover, the relationships using each of the 3 alternative definitions of ALCSD relative to RNFLT appeared to be similar, and the interaction term (RNFLT × Age) for each definition achieved a similar level of significance ($ALCSD_{max1}$, $P = 0.081$; $ALCSD_{max2}$, $P = 0.074$; $ALCSD_{central}$, $P = 0.085$).

Discussion

Our findings suggest that older eyes have a lamina that is shallower than younger eyes at a given level of VF loss and that this age-related difference increases with advancing disease severity (i.e., for each dB of VF damage). These findings were consistent across a variety of laminar depth parameters and were also present when RNFLT rather than MD was used as a measure of "disease stage."

Rho et al.[55] reported age-related differences in laminar displacement in 8 of 12 clock-hour positions in 26 eyes of 26 primary open-angle glaucoma (POAG) patients but interestingly found no age-related differences in laminar displacement among 52 eyes of 52 normal tension glaucoma patients. Similar

Investigative Ophthalmology & Visual Science

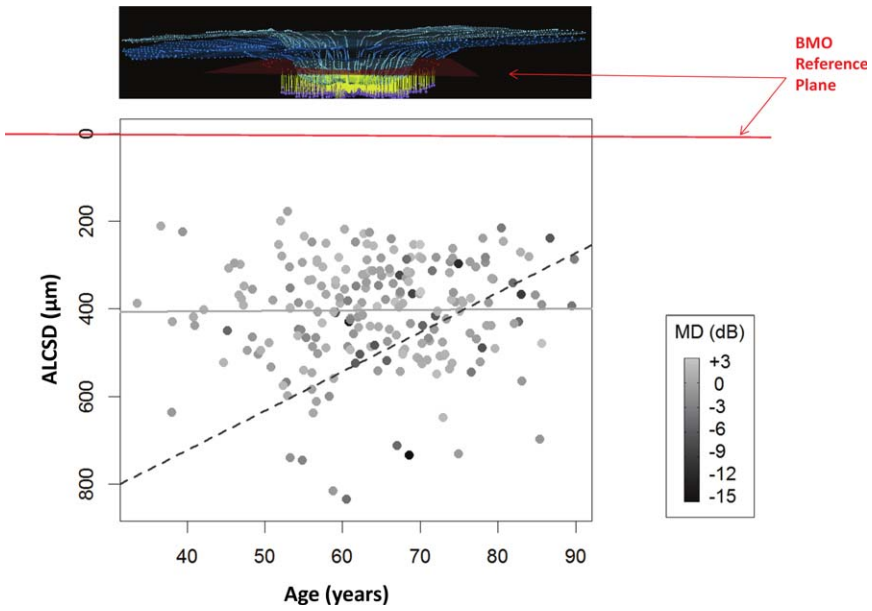

Figure 5. The relationship between ALCSD and age is shown, with points shaded according to their VF MD. The regression equation for ALCSD was: ALCSD = 407.68 − 67.13 × MD − 0.08 × Age + 0.89 × MD × Age (MD, $P = 0.001$; age, $P = 0.921$; MD × age, $P = 0.004$). Each point is shaded by the value of the MD, with the darkest being the lowest MD values (continuous scale to the *right*). By our convention, ALCSD as a parameter becomes greater as the distance between the ALCS and the BMO reference plane increases (Fig. 3). Two regression lines are shown, based on the equation given above: the relationship between ALCSD and age for MD = 0 dB (*solid gray line*), and the relationship for MD = −10 dB (*dashed gray line*). For a given amount of damage (or worse MD), the ALCS is deeper in younger eyes than in older eyes. Note that most cases with worse VF status (*darker colored dots*) are located in the *upper right* portion of the distribution, that is, in older eyes with shallower ALCSD.

to our study, they adjusted their comparisons for severity of VF damage and IOP at presentation. Unlike our study, they found direct (negative) correlations between age and laminar position in the POAG subgroup and hypothesized that the low levels of IOP at which normal tension glaucoma occurs and progresses did not allow for age-related differences in laminar stiffness to be clinically manifested within the normal tension glaucoma group.

The hypothesis that the structural stiffness of the ONH and peripapillary scleral connective tissues contribute to an individual eye's structure/function association is important because it leads to predictions that can be tested longitudinally in young eyes (or compliant eyes of all ages) and in old eyes (or stiff eyes of all ages). For example, in eyes that have similar levels of detected IOP exposure, is ONH structural progression more likely to precede RNFL and/or VF progression in

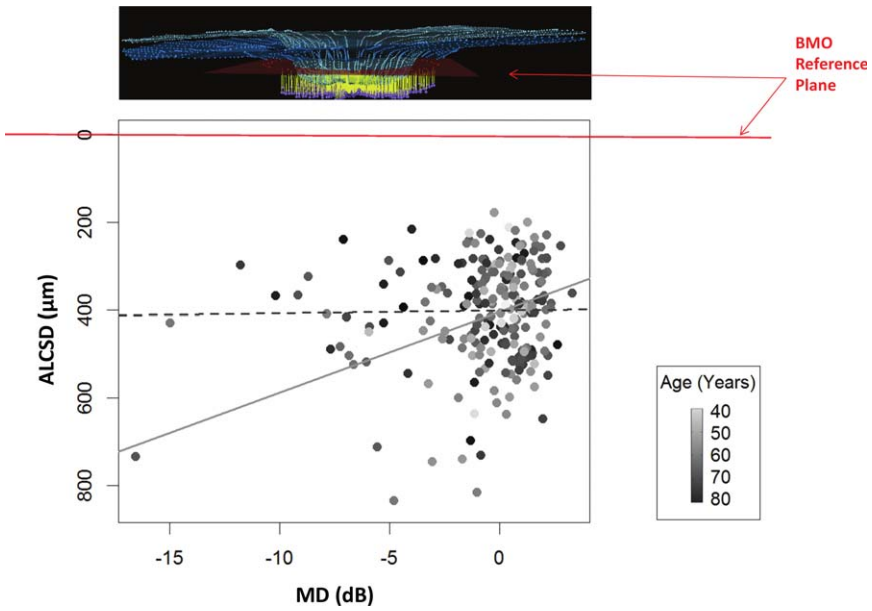

Figure 6. The relationship between ALCSD and VF MD is shown, with points shaded according to their age. Each point is shaded by age, with the darkest being the oldest age values (continuous scale to the *right*). Two regression lines are shown, based on the same equation as given in Figure 5: the relationship between ALCSD and MD at age 55 (*solid gray line*) and the relationship at age 75 (*dashed gray line*). For younger subjects, the ALCS is deeper in more damaged eyes. For older subjects, the surface depth is unrelated to the amount of damage.

Investigative Ophthalmology & Visual Science

compliant as compared with stiff eyes? Conversely, is detectable VF and/or RNFL change more likely to precede detectable ONH structural change in stiff versus compliant eyes?

If ONH structure/function relationships are eye-specific, it will be due in part to the fact that ONH structural change includes multiple components, each of which may contribute variably to RGC axon damage and eventual functional loss. Reversible conformational change or deformation of the neural and connective tissues that does not harm the adjacent RGC axons may occur at all levels of IOP depending upon the compliance of the ONH tissues.[56,57] Connective tissue remodeling[38,39] in response to IOP- and non-IOP-related stimuli should result in permanent (irreversible) change and may protect or insult the adjacent axons.[15] RGC axon cytoarchitectural disruption[58,59] may be reversible and precede RGC axon damage and loss. Finally, RGC axon loss, by whatever mechanism, may be related to functional loss in a variable manner, depending upon the test.[60]

It has been suggested that structure/function relationships in glaucoma change with age.[26,61] Our data additionally suggest that if there are age-related differences in structure/function associations, there may be multiple mechanisms by which these occur.

Our study has the following limitations. First, the fact that we found no significant univariate association between IOP and ALCSD or RNFLT may be due to the fact that our IOP characterization relied on a single IOP measurement during regular clinic hours performed closest to the SDOCT scan date. IOP is a dynamic parameter with distinct circadian rhythms that vary among individuals. There is evidence that single IOP measurements during regular clinic hours fail to reflect the true range of an individual's IOP.[62] Studies that evaluate 24-hour IOP in glaucoma patients have found that two-thirds of patients exhibit their highest IOP values outside regular clinic hours, most frequently during nocturnal/sleep period.[63–65]

In addition to the lack of a complete IOP characterization at the time it was measured, the IOP risk factor is likely to be most important to the hypotheses we tested is some measure of the cumulative IOP insult that occurred in each eye over the full period in which the structural and functional changes we characterized had occurred. Such a characterization is not possible for several reasons. It would require knowing the point at which the neuropathy started in each study eye; accurate telemetric characterization of IOP magnitude and fluctuation over the entire course of the neuropathy; and knowing the relative contributions of IOP magnitude and IOP fluctuation to IOP insult.

Second, the measure of functional VF status used (MD) was corrected for age and may therefore be a good indicator of the amount of glaucomatous damage (given the strict exclusion criteria). However our measurements of ALCSD and RNFLT were not corrected for age and thus only indirectly reflect damage. Prospective longitudinal studies are required that directly measure the magnitude of ALCSD, RNFLT, and MD change over time.

Third, this study used standard SDOCT rather than enhanced depth imaging, which might have provided a more accurate characterization of ALCSD.[48,66,67] Our previous study[47] provided histologic verification of standard SDOCT ALCS delineation. In the present study, using standard SDOCT, the percentage of ALCS sectors that achieved our criteria for visualization ranged from 18% to 100% (median, 54%) with most eyes achieving greater than 50% visualization.

Axial length was not measured in our study participants. Its use might have allowed us to more accurately correct for eye-specific transverse magnification. As a result, the location of the RNFLT measurements in each eye might not have been as consistent among all study eyes, although the magnitude of this effect should be limited by the range of accepted refractive errors. Because SDOCT measurements in the z-axis should not require magnification correction, our measurements of ALCSD and RNFLT should have been only minimally affected both because we excluded eyes with spectacle refraction equal to or greater than ±5.00-D sphere and equal to or greater than ±2.00-D cylinder, and only the transverse component of our ALCSD and RNFLT measurements would require correction.

Finally, this is a cross-sectional study that detected an effect of age which we hypothesized to be related to laminar stiffness. However, the contribution of age and ONH structural stiffness to the clinical manifestation of glaucomatous damage needs to be determined within longitudinal studies of compliant and stiff eyes of all ages that have been matched for similar levels of cumulative IOP exposure and glaucomatous damage.

In summary, the results of this cross-sectional study are consistent with the concept that glaucomatous structure/structure and structure/function relationships change with age. In younger eyes, laminar position was deeper in eyes with more pronounced VF loss, whereas in older eyes, laminar position was independent of VF MD.

Acknowledgments

The authors thank Juan Reynaud, Cindy Blachly, and Michael Whitworth for their SDOCT technical support (JR) and clinical imaging of the P3 participants (CB and MW). We also thank Joanne Couchman for assistance with manuscript preparation and submission.

Presented in part at the annual meeting of the American Glaucoma Society, New York, New York, March 2012, and at the Annual Meeting of the Association for Research in Vision and Ophthalmology, Fort Lauderdale, Florida, May 2012.

Supported by National Institutes of Health (NIH)/National Eye Institute (NEI) Grant R01-EY-019674 (SD); Legacy Good Samaritan Foundation; Carl Zeiss Meditec; NIH/NEI Grant R01-EY021281 (CFB); and Heidelberg Engineering, GmbH, Heidelberg, Germany. Claude F. Burgoyne is a consultant to Heidelberg Engineering. The above listed sponsors/funding organizations had no role in the design or conduct of this research. The authors alone are responsible for the content and writing of the paper.

Disclosure: **R. Ren**, None; **H. Yang**, None; **S.K. Gardiner**, None; **B. Fortune**, Carl Zeiss Meditec (F), Heidelberg Engineering (F); **C. Hardin**, None; **S. Demirel**, Legacy Good Samaritan Foundation (F), Carl Zeiss Meditec (F); **C.F. Burgoyne**, Legacy Good Samaritan Foundation (F), Heidelberg Engineering (F, C, R)

References

1. Quigley HA. Open-angle glaucoma. *N Engl J Med*. 1993;328:1097–1106.
2. Tielsch JM, Sommer A, Katz J, Royall RM, Quigley HA, Javitt J. Racial variations in the prevalence of primary open-angle glaucoma. The Baltimore Eye Survey. *JAMA*. 1991;266:369–374.
3. Gordon MO, Beiser JA, Brandt JD, et al. The Ocular Hypertension Treatment Study: baseline factors that predict the onset of primary open-angle glaucoma. *Arch Ophthalmol*. 2002;120:714–720; discussion 829–830.
4. Heijl A, Leske MC, Bengtsson B, Hussein M. Measuring visual field progression in the Early Manifest Glaucoma Trial. *Acta Ophthalmol Scand*. 2003;81:286–293.
5. Nouri-Mahdavi K, Hoffman D, Coleman AL, et al. Predictive factors for glaucomatous visual field progression in the Advanced Glaucoma Intervention Study. *Ophthalmology*. 2004;111:1627–1635.

6. Jonas JB, Grundler A. Optic disc morphology in "age-related atrophic glaucoma." *Graefes Arch Clin Exp Ophthalmol*. 1996;234:744–749.
7. Geijssen HC, Greve EL. The spectrum of primary open angle glaucoma. I: Senile sclerotic glaucoma versus high tension glaucoma. *Ophthalmic Surg*. 1987;18:207–213.
8. Broadway DC, Nicolela MT, Drance SM. Optic disk appearances in primary open-angle glaucoma. *Surv Ophthalmol*. 1999;43(suppl 1):S223–S243.
9. Nicolela MT, Drance SM, Broadway DC, Chauhan BC, McCormick TA, LeBlanc RP. Agreement among clinicians in the recognition of patterns of optic disk damage in glaucoma. *Am J Ophthalmol*. 2001;132:836–844.
10. Nicolela MT, Drance SM. Various glaucomatous optic nerve appearances: clinical correlations. *Ophthalmology*. 1996;103:640–649.
11. Nicolela MT, McCormick TA, Drance SM, Ferrier SN, LeBlanc RP, Chauhan BC. Visual field and optic disc progression in patients with different types of optic disc damage: a longitudinal prospective study. *Ophthalmology*. 2003;110:2178–2184.
12. Nicolela MT, Walman BE, Buckley AR, Drance SM. Various glaucomatous optic nerve appearances. A color Doppler imaging study of retrobulbar circulation. *Ophthalmology*. 1996;103:1670–1679.
13. Jonas JB, Grundler A. Optic disc morphology in juvenile primary open-angle glaucoma. *Graefes Arch Clin Exp Ophthalmol*. 1996;234:750–754.
14. Burgoyne CF, Downs JC. Premise and prediction—how optic nerve head biomechanics underlies the susceptibility and clinical behavior of the aged optic nerve head. *J Glaucoma*. 2008;17:318–328.
15. Burgoyne CF. A biomechanical paradigm for axonal insult within the optic nerve head in aging and glaucoma. *Exp Eye Res*. 2011;93:120–132.
16. Albon J, Purslow PP, Karwatowski WS, Easty DL. Age related compliance of the lamina cribrosa in human eyes. *Br J Ophthalmol*. 2000;84:318–323.
17. Albon J, Farrant S, Akhtar S, et al. Connective tissue structure of the tree shrew optic nerve and associated ageing changes. *Invest Ophthalmol Vis Sci*. 2007;48:2134–2144.
18. Albon J, Karwatowski WS, Avery N, Easty DL, Duance VC. Changes in the collagenous matrix of the aging human lamina cribrosa. *Br J Ophthalmol*. 1995;79:368–375.
19. Albon J, Karwatowski WS, Easty DL, Sims TJ, Duance VC. Age related changes in the non-collagenous components of the extracellular matrix of the human lamina cribrosa. *Br J Ophthalmol*. 2000;84:311–317.
20. Bailey AJ, Paul RG, Knott L. Mechanisms of maturation and ageing of collagen. *Mech Ageing Dev*. 1998;106:1–56.
21. Brown CT, Vural M, Johnson M, Trinkaus-Randall V. Age-related changes of scleral hydration and sulfated glycosaminoglycans. *Mech Ageing Dev*. 1994;77:97–107.
22. Friedenwald J. Contribution to the theory and practice of tonometry. *Am J Ophthalmol*. 1937;20:985–1024.
23. Hernandez MR, Luo XX, Andrzejewska W, Neufeld AH. Age-related changes in the extracellular matrix of the human optic nerve head. *Am J Ophthalmol*. 1989;107:476–484.
24. Kotecha A, Izadi S, Jeffrey G. Age related changes in the thickness of the human lamina cribrosa. *Br J Ophthalmol*. 2006;90:1531–1534.
25. Morrison JC, Jerdan JA, Dorman ME, Quigley HA. Structural proteins of the neonatal and adult lamina cribrosa. *Arch Ophthalmol*. 1989;107:1220–1224.
26. Harwerth RS, Wheat JL, Fredette MJ, Anderson DR. Linking structure and function in glaucoma. *Prog Retin Eye Res*. 2010;29:249–271.
27. Emery JM, Landis D, Paton D, Boniuk M, Craig JM. The lamina cribrosa in normal and glaucomatous human eyes. *Trans Am Acad Ophthalmol Otolaryngol*. 1974;78:OP290–297.
28. Quigley HA, Addicks EM, Green WR, Maumenee AE. Optic nerve damage in human glaucoma. II. The site of injury and susceptibility to damage. *Arch Ophthalmol*. 1981;99:635–649.
29. Quigley HA, Hohman RM, Addicks EM, Massof RW, Green WR. Morphologic changes in the lamina cribrosa correlated with neural loss in open-angle glaucoma. *Am J Ophthalmol*. 1983;95:673–691.
30. Bellezza AJ, Rintalan CJ, Thompson HW, Downs JC, Hart RT, Burgoyne CF. Deformation of the lamina cribrosa and anterior scleral canal wall in early experimental glaucoma. *Invest Ophthalmol Vis Sci*. 2003;44:623–637.
31. Jonas JB, Berenshtein E, Holbach L. Anatomic relationship between lamina cribrosa, intraocular space, and cerebrospinal fluid space. *Invest Ophthalmol Vis Sci*. 2003;44:5189–5195.
32. Burgoyne CF, Downs JC, Bellezza AJ, Hart RT. Three-dimensional reconstruction of normal and early glaucoma monkey optic nerve head connective tissues. *Invest Ophthalmol Vis Sci*. 2004;45:4388–4399.
33. Downs JC, Yang H, Girkin C, et al. 3-D Histomorphometry of the normal and early glaucomatous monkey optic nerve head: neural canal and subarachnoid space architecture. *Invest Ophthalmol Vis Sci*. 2007;48:3195–3208.
34. Yang H, Downs JC, Bellezza AJ, Thompson H, Burgoyne CF. 3-D Histomorphometry of the normal and early glaucomatous monkey optic nerve head: prelaminar neural tissues and cupping. *Invest Ophthalmol Vis Sci*. 2007;48:5068–5084.
35. Yang H, Downs JC, Girkin C, et al. 3-D Histomorphometry of the normal and early glaucomatous monkey optic nerve head: lamina cribrosa and peripapillary scleral position and thickness. *Invest Ophthalmol Vis Sci*. 2007;48:4597–4607.
36. Yang H, Downs JC, Sigal IA, Roberts MD, Thompson H, Burgoyne CF. Deformation of the normal monkey optic nerve head connective tissue after acute IOP elevation within 3-D histomorphometric reconstructions. *Invest Ophthalmol Vis Sci*. 2009;50:5785–5799.
37. Yang H, Thompson H, Roberts MD, Sigal IA, Downs JC, Burgoyne CF. Deformation of the early glaucomatous monkey optic nerve head connective tissue after acute IOP elevation in 3-D histomorphometric reconstructions. *Invest Ophthalmol Vis Sci*. 2011;52:345–363.
38. Roberts MD, Grau V, Grimm J, et al. Remodeling of the connective tissue microarchitecture of the lamina cribrosa in early experimental glaucoma. *Invest Ophthalmol Vis Sci*. 2009;50:681–690.
39. Yang H, Williams G, Downs JC, et al. Posterior (outward) migration of the lamina cribrosa and early cupping in monkey experimental glaucoma. *Invest Ophthalmol Vis Sci*. 2011;52:7109–7121.
40. Hernandez MR, Miao H, Lukas T. Astrocytes in glaucomatous optic neuropathy. *Prog Brain Res*. 2008;173:353–373.
41. Bellezza AJ, Rintalan CJ, Thompson HW, Downs JC, Hart RT, Burgoyne CF. Anterior scleral canal geometry in pressurised (IOP 10) and non-pressurised (IOP 0) normal monkey eyes. *Br J Ophthalmol*. 2003;87:1284–1290.
42. Sigal IA, Yang H, Roberts MD, Burgoyne CF, Downs JC. IOP-induced lamina cribrosa displacement and scleral canal expansion: an analysis of factor interactions using parameterized eye-specific models. *Invest Ophthalmol Vis Sci*. 2010;52:1896–1907.
43. Sigal IA, Yang H, Roberts MD, et al. IOP-induced lamina cribrosa deformation and scleral canal expansion: independent or related? *Invest Ophthalmol Vis Sci*. 2011;52:9023–9032.
44. Drexler W, Fujimoto JG. State-of-the-art retinal optical coherence tomography. *Prog Retin Eye Res*. 2008;27:45–88.

Investigative Ophthalmology & Visual Science

45. Inoue R, Hangai M, Kotera Y, et al. Three-dimensional high-speed optical coherence tomography imaging of lamina cribrosa in glaucoma. *Ophthalmology*. 2009;116:214–222.
46. Strouthidis NG, Fortune B, Yang H, Sigal IA, Burgoyne CF. Longitudinal change detected by spectral domain optical coherence tomography in the optic nerve head and peripapillary retina in experimental glaucoma. *Invest Ophthalmol Vis Sci*. 2011;52:1206–1219.
47. Strouthidis NG, Grimm J, Williams G, Cull G, Wilson DJ, Burgoyne CFA. Comparison of optic nerve head morphology viewed by spectral domain optical coherence tomography and by serial histology. *Invest Ophthalmol Vis Sci*. 2010;51:1464–1474.
48. Lee EJ, Kim TW, Weinreb RN, Park KH, Kim SH, Kim DO. Visualization of the lamina cribrosa using enhanced depth imaging spectral-domain optical coherence tomography. *Am J Ophthalmol*. 2011;152:87–95. e81.
49. Gardiner SK, Johnson CA, Demirel S. Factors predicting the rate of functional progression in early and suspected glaucoma. *Invest Ophthalmol Vis Sci*. 2012;53:3598–3604.
50. Bengtsson B, Olsson J, Heijl A, Rootzen H. A new generation of algorithms for computerized threshold perimetry, SITA. *Acta Ophthalmol Scand*. 1997;75:368–375.
51. Heidelberg Engineering. Spectralis Operating Instructions. Version 001 ed. Heidelberg, Germany; 2007.
52. Yang H, Qi J, Hardin C, et al. Spectral-domain optical coherence tomography enhanced depth imaging of the normal and glaucomatous nonhuman primate optic nerve head. *Invest Ophthalmol Vis Sci*. 2012;53:394–405.
53. Strouthidis NG, Yang H, Fortune B, Downs JC, Burgoyne CF. Detection of optic nerve head neural canal opening within histomorphometric and spectral domain optical coherence tomography data sets. *Invest Ophthalmol Vis Sci*. 2009;50:214–223.
54. Fortune B, Yang H, Strouthidis NG, et al. The effect of acute intraocular pressure elevation on peripapillary retinal thickness, retinal nerve fiber layer thickness and retardance. *Invest Ophthalmol Vis Sci*. 2009;50:4719–4726.
55. Rho CR, Park HY, Lee NY, Park CK. Clock-hour laminar displacement and age in primary open-angle glaucoma and normal tension glaucoma. *Clin Experiment Ophthalmol*. 2012;40:e183–189.
56. Quigley HA. Childhood glaucoma: results with trabeculotomy and study of reversible cupping. *Ophthalmology*. 1982;89:219–226.
57. Reis AS, O'Leary N, Stanfield MJ, Shuba LM, Nicolela MT, Chauhan BC. Laminar displacement and prelaminar tissue thickness change after glaucoma surgery imaged with optical coherence tomography. *Invest Ophthalmol Vis Sci*. 2012;53:5819–5826.
58. Fortune B, Burgoyne CF, Cull GA, Reynaud J, Wang L. Structural and functional abnormalities of retinal ganglion cells measured in vivo at the onset of optic nerve head surface change in experimental glaucoma. *Invest Ophthalmol Vis Sci*. 2012;53:3939–3950.
59. Huang XR, Knighton RW. Altered F-actin distribution in retinal nerve fiber layer of a rat model of glaucoma. *Exp Eye Res*. 2009;88:1107–1114.
60. Gardiner SK, Johnson CA, Demirel S. The effect of test variability on the structure-function relationship in early glaucoma. *Graefes Arch Clin Exp Ophthalmol*. 2012;250:1851–1861.
61. Harwerth RS, Wheat JL, Rangaswamy NV. Age-related losses of retinal ganglion cells and axons. *Invest Ophthalmol Vis Sci*. 2008;49:4437–4443.
62. Barkana Y, Anis S, Liebmann J, Tello C, Ritch R. Clinical utility of intraocular pressure monitoring outside of normal office hours in patients with glaucoma. *Arch Ophthalmol*. 2006;124:793–797.
63. Liu JH, Kripke DF, Twa MD, et al. Twenty-four-hour pattern of intraocular pressure in the aging population. *Invest Ophthalmol Vis Sci*. 1999;40:2912–2917.
64. Liu JH, Weinreb RN. Monitoring intraocular pressure for 24 h. *Br J Ophthalmol*. 2011;95:599–600.
65. Liu JH, Zhang X, Kripke DF, Weinreb RN. Twenty-four-hour intraocular pressure pattern associated with early glaucomatous changes. *Invest Ophthalmol Vis Sci*. 2003;44:1586–1590.
66. Park HY, Jeon SH, Park CK. Enhanced depth imaging detects lamina cribrosa thickness differences in normal tension glaucoma and primary open-angle glaucoma. *Ophthalmology*. 2012;119:10–20.
67. Park SC, De Moraes CG, Teng CC, Tello C, Liebmann JM, Ritch R. Enhanced depth imaging optical coherence tomography of deep optic nerve complex structures in glaucoma. *Ophthalmology*. 2012;119:3–9.

Investigative Ophthalmology & Visual Science